



HAL
open science

Determination of orientation relationships between FCC-hydride and HCP-titanium and their correlation with hydrides distribution

Jing Wen, Nathalie Allain, Eric Fleury

► **To cite this version:**

Jing Wen, Nathalie Allain, Eric Fleury. Determination of orientation relationships between FCC-hydride and HCP-titanium and their correlation with hydrides distribution. *Journal of Alloys and Compounds*, 2020, 817, pp.153297. 10.1016/j.jallcom.2019.153297 . hal-02534639

HAL Id: hal-02534639

<https://hal.univ-lorraine.fr/hal-02534639>

Submitted on 7 Apr 2020

HAL is a multi-disciplinary open access archive for the deposit and dissemination of scientific research documents, whether they are published or not. The documents may come from teaching and research institutions in France or abroad, or from public or private research centers.

L'archive ouverte pluridisciplinaire **HAL**, est destinée au dépôt et à la diffusion de documents scientifiques de niveau recherche, publiés ou non, émanant des établissements d'enseignement et de recherche français ou étrangers, des laboratoires publics ou privés.

Determination of orientation relationships between FCC-hydride and HCP-titanium and their correlation with hydrides distribution

Jing WEN*, Nathalie ALLAIN, Eric FLEURY*

Université de Lorraine, CNRS, Arts et Métiers ParisTech, LEM3, F-57000 Metz, France

Abstract

Since the crystallographic orientation relationships (ORs) play an important role in the hydrides precipitation as well as in the deformation behavior of α -titanium alloys containing hydrides, the present work aimed at exploring thoroughly the ORs and their interface planes between the fcc-hydride and the α -titanium using the stereographic projections of the corresponding OR plane and OR direction and a trace analysis. In addition to the general reported two ORs in the α -titanium, a new OR closely related to the texture component of the rolled Ti-sheet is also determined in the present work. The overall identified ORs and their interface planes are accounted for by edge-to-edge matching model. Furthermore, a quantitative analysis using the high-angular resolution SEM-EBSD highlighted the dependency of hydride distribution on the ORs and the parent grain orientation.

Keywords: Titanium hydride; Orientation relationships; interface planes; Electron backscatter diffraction; Grain orientation

Corresponding authors:

Dr. Jing Wen, currently a postdoc at Institut Néel and UGA, email: jing.wen@neel.cnrs.fr

Prof. Eric Fleury, email: eric.fleury@univ-lorraine.fr

1. Introduction

Due to an attractive combination of mechanical and chemical properties [1, 2], the commercially pure titanium Ti50A (ASTM Grade 2) have become promising candidates in the field of chemical industry, marine and biomedical materials. In most of these applications, the components are unavoidably exposed to environments that can act as sources of hydrogen [3]. The fast diffusion and the low solubility limit of hydrogen in the hcp lattice at ambient temperature enable the formation of titanium-hydride in α -Ti alloys even at a low hydrogen concentration [4-6]. For example, the studies of Banerjee et al. [7], Van Heerden et al. [8], and Casanove et al. [9] have shown that titanium hydrides can form during sample thinning

used for the preparation of thin foils for transmission electron microscopy (TEM) observation. Since hydrides are generally considered as detrimental phases to titanium and its alloys owing to its brittle nature causing embrittlement and rupture, understanding the formation of titanium hydrides with examination of the crystallographic orientation is critical to control and predict the properties and performance of titanium products operating under hydrogen (H_2 , H and H^+) atmospheres.

According to the Ti-H phase diagram [10], three types of hydride phases possessing different crystal structures are formed depending on the hydrogen concentration: γ -TiH (face-centered tetragonal), δ -TiH_{2-x} (face-centered cubic) with x ranging between 0 and 0.4) and ϵ -TiH₂ (body-centered tetragonal) [11, 12]. The nature of these hydride phases is dependent on the hydrogen content, but also on their crystallographic orientation relationship (OR) with the matrix α -phase [5]. The ORs between hydride phases and titanium matrix have been investigated in recent studies by means of TEM characterization. Two ORs referred as **OR1** ($\{0001\}_\alpha // \{001\}_\delta$ & $\langle 11\bar{2}0 \rangle_\alpha // \langle 110 \rangle_\delta$) and **OR2** ($\{0001\}_\alpha // \{\bar{1}11\}_\gamma$, angle of 4° & $\langle 11\bar{2}0 \rangle_\alpha // \langle 110 \rangle_\gamma$) have been frequently observed in α -Ti alloys [4-7, 11-15]. According to the work of Conforto et al. [4-6], the formation of the stable δ -hydride occurs either directly at the TiH_{2-x}/Ti interface owing to a favorable crystallographic OR, or through the formation of the intermediate hydride phase γ -TiH (γ -TiH \rightarrow δ -TiH_{2-x}) without changing their OR with the matrix α -phase.

On the other hand, TEM observations particularly dedicated to the study of the interaction of hydrides with dislocations or twins revealed that the transfer of deformation (dislocation slip or twinning) across the hydride is not dependent on the type of hydride (γ or δ) but rather on the crystallographic orientation relationships between the α -matrix and the hydrides [16-20]. Based on these previous studies, the crystallographic orientation relationships are believed to play a major role in the hydride precipitation but also in the deformation behavior of α -titanium alloys containing hydrides. Therefore, the present work aimed at exploring thoroughly the ORs in electrolytically charged commercially pure Ti and conducting a quantitative analysis of their dependency with the grain orientation using high-angular resolution electron backscatter diffraction (EBSD) technique. In contrast to studies performed in TEM, EBSD-based analyses avoid artefacts caused by thin foil specimen preparation [7-9]. Additionally, EBSD scan can be carried out at a larger scale, revealing the spatial patterning in crystal structures over a large number of contiguous grains [21].

2. Method

This study has been undertaken using commercially pure titanium Ti50A in the form of 1.60 mm thick sheet in the annealed state purchased from TIMET. The thickness of the as-received (AR) sheets were reduced to around 1.0 mm by mechanical polishing using successively 300, 500, 1000, 2000 and 4000 SiC paper grits followed by an annealing treatment performed under vacuum for 2 h at 350 °C to relieve the potential residual stresses generated during sample preparation. With the aim of minimizing the undesired factors such as surface layers and/or residual stresses that could have significant effect on the hydrogen evolution, the samples received a final vibrating polishing for 2 h. Hydrogen was introduced into the specimens by an electrolytic method. A mesh-type platinum anode of cylindrical shape was used, and the specimen was located in the center of the electrolytic cell as described in ref. [22]. Specimens ($50 \times 15 \times 1.0\text{mm}^3$) were charged with hydrogen in an electrolyte consisting of 1/3 phosphoric acid (85%) and 2/3 glycerin (85%) [23] under an applied current density of 2 mA/cm^2 for 168 h. The amount of hydrogen dissolved in the sample was reported in Ref. [24].

The transformations from titanium into titanium hydride were inspected using the combined X-ray diffraction (XRD) and scanning electron microscopy (SEM)-EBSD analyses. The XRD measurements were undertaken using Cu-K α radiation with a wavelength of 0.154 nm. To index qualitatively EBSD patterns (Kikuchi patterns), the samples were electropolished at 5 °C and 30 V for 10 s in a solution of 100 ml perchloric acid and 900 ml methanol. The microstructure developed through hydrogen charging was examined using a JEOL-6500F field emission gun SEM equipped with an EBSD acquisition camera and the AZtec acquisition software package at a step size of 0.15 μm . Since EBSD measurement provided the Euler angles (ϕ_1, Φ, ϕ_2) of each pixel, the crystallographic ORs represented by the stereographic projections of the corresponding OR plane and OR direction of the two phases, were determined using the rotation matrix written in MatLab software [25, 26].

3. Results and discussion

3.1 Distribution characteristics of hydrides in the hydrogenated Ti50A-H

Fig. 1 presents the microstructure of the annealed Ti50A characterized by the EBSD maps and pole figures $\{0002\}$ and $\{10-10\}$. As revealed by the inverse pole figure (IPF) map superimposed with grain boundaries (Fig. 1a), the microstructure of the annealed Ti50A is composed of equiaxed grains with a mean grain size of about $12 \pm 0.8 \mu\text{m}$ (3500 grains). No internal structure was observed in the interior of α grains, whereas the occurrence of α grains

having a preferential orientation (texture) with respect to the normal direction (ND) was frequently noticed. EBSD phase map superimposed with grain boundary (Fig. 1b) highlighted the presence of a unique α phase contained in hydrogen-free as-received Ti50A (referred as AR-Ti50A). Fig. 1c shows the $\{0002\}$ pole figure of the annealed Ti50A characterized by a TD-split basal texture with a maximum intensity occurring at $\pm 30^\circ$ tilted from the ND to the TD. Such a texture is typical for hot rolled Ti50A sheets, which cannot be totally removed by the subsequent annealing treatment.

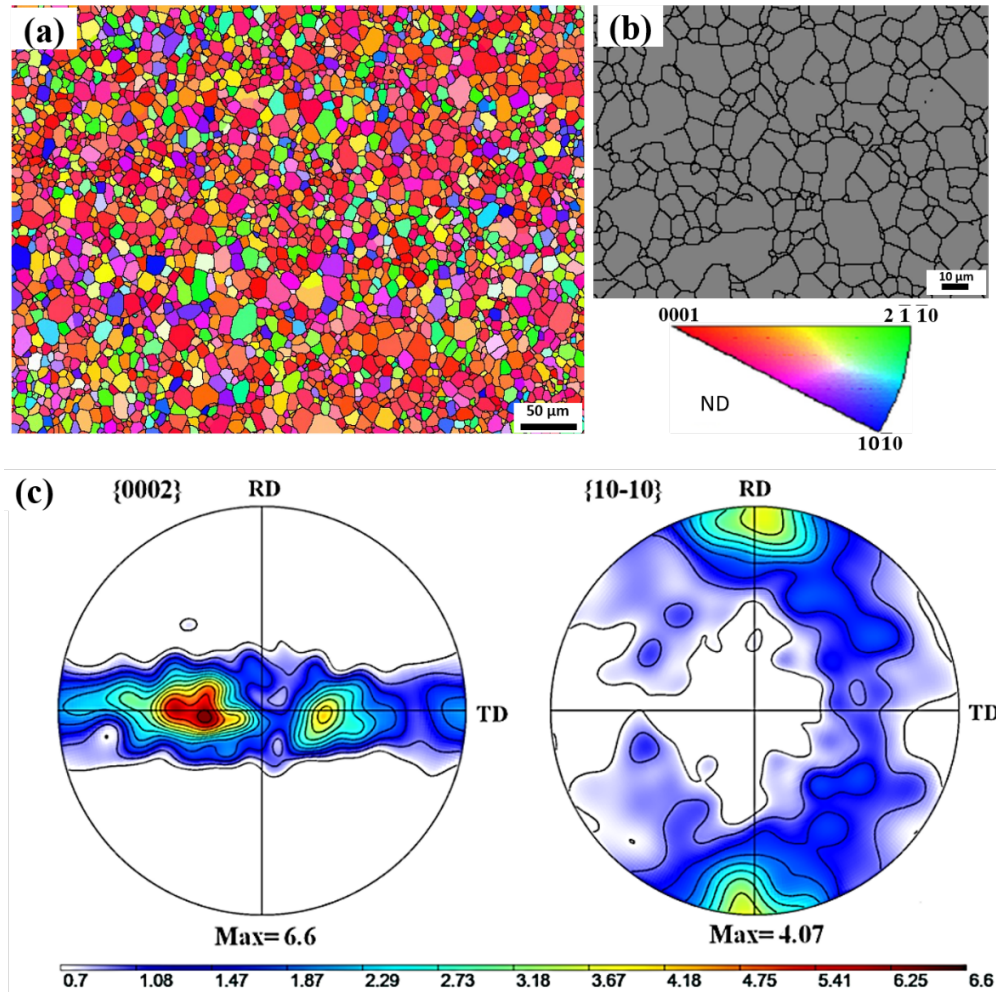


Fig. 1 Initial microstructure of Ti50A revealed by EBSD. (a) Inverse Pole Figure (IPF) map, (b) phase map superimposed with grain boundaries and (c) pole figure of plane $\{0002\}$ and $\{10\bar{1}0\}$, respectively.

Fig. 2a gives the XRD patterns of the AR-Ti50A as well as that of a Ti50A sample hydrogenated for 168h (referred as Ti50A-H). The hydrogen-free AR-Ti50A displayed a single diffraction pattern corresponding to the α phase, whereas that of the Ti50A-H is characterized by the superimposition of three series of spectrums indicating the precipitation of additional phases. Further analyses of the diffraction pattern of Ti50A-H evidenced the precipitation of two types of titanium hydrides, i.e., δ -TiH_{2-x} and ϵ -TiH₂. The δ -TiH_{2-x} ($0 \leq$

$x \leq 0.4$) hydride has an FCC lattice ($a = 0.4445 \text{ nm}$) with the hydrogen atoms occupying the tetrahedral interstitial sites (CaF_2 structure) [27], while the $\epsilon\text{-TiH}_2$ hydride has a body-centered tetragonal (BCT) lattice with $a = 0.312 \text{ nm}$ and $c = 0.418 \text{ nm}$ [28]. As noticed, the intensity of the diffraction peak $(002)_\epsilon$ (which solely accounts for the $\epsilon\text{-TiH}_2$ hydride) is barely visible as the hydrogen charging time increased to 168 h. Indeed, the structure of $\epsilon\text{-TiH}_2$ hydride is unstable, it could transform into the stable $\delta\text{-TiH}_{2-x}$ hydride above 310k [29], as discussed in the previous work [24]. In addition, it can be noticed that the XRD peaks corresponding to the matrix α -phase became broadened for the Ti50A-H. As pointed by Williams et al. [30], these broadened diffraction peaks can be attributed to the occurrence of local plastic deformation associated with the volume expansion (around 15%) caused by the hydride precipitation.

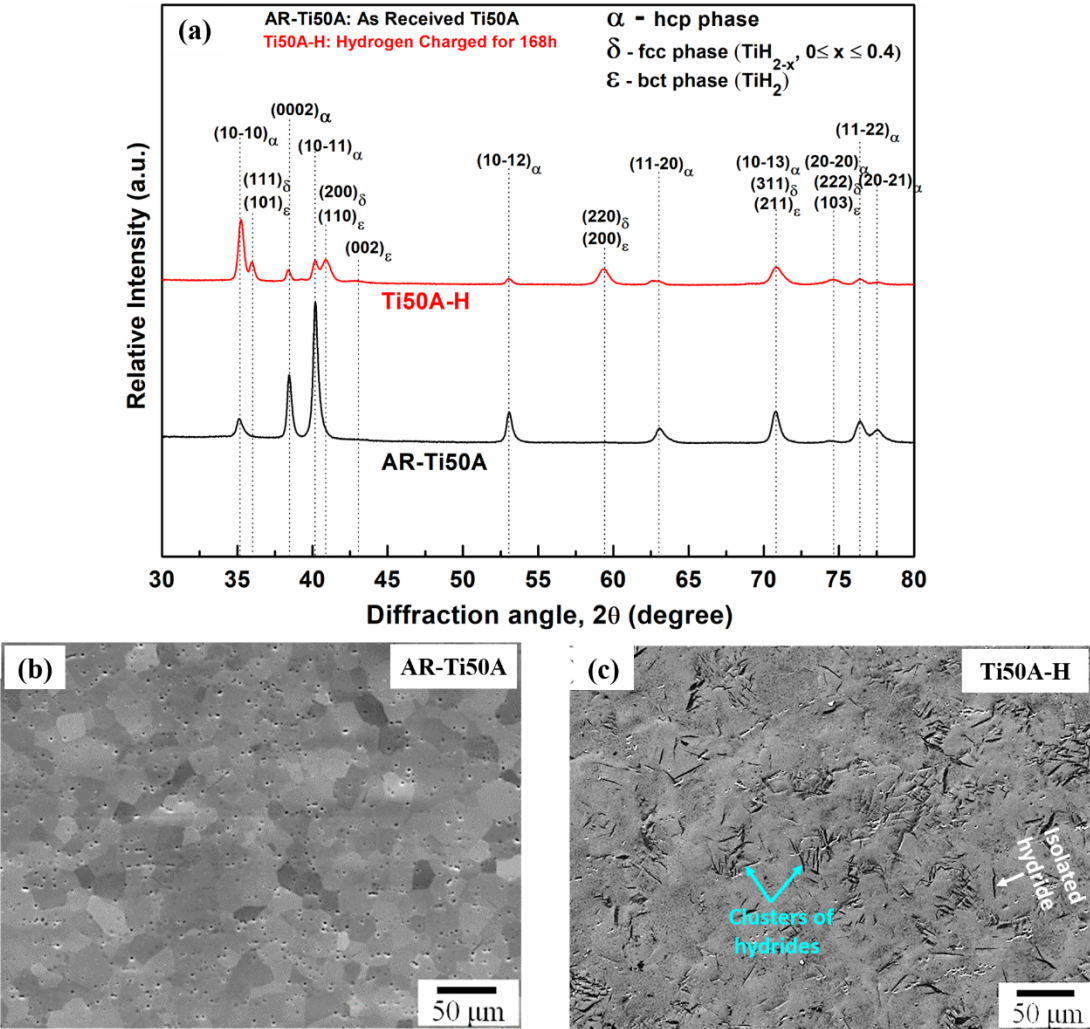


Fig. 2 Microstructural characterization of the as received (AR-Ti50A) and the hydrogenated Ti50A-H (hydrogen charged for 168 h) samples. (a) XRD patterns; (b) SEM-SEI of AR-Ti50A and (c) SEM-SEI image of Ti50A-H (two characteristics of hydride distribution: the isolated hydride and the cluster of hydrides indicated by white and green arrow, respectively.)

Fig. 2b and c show the secondary electron images (SEI) of AR-Ti50A and hydrogenated sample Ti50A-H, respectively. Consistent with the EBSD characterization in Fig. 1a and b, only the α phase and no other phases are present in AR-Ti50A. In contrast to the hydrogen-free AR-Ti50A sample, the hydrogenated Ti50A-H sample displays a plate-like morphology (Fig. 2c). As seen, hydrides are either observed isolated or grouped to form cluster of small sized hydrides, the thickness of hydrides varied from tens of nanometers to hundreds of nanometers, as outlined in Fig. 2c. The observation of heterogeneously distributed hydrides throughout the sample suggested that the precipitation of hydrides could be related to the orientation of the α -grain. The correlation between the hydride precipitation and grain orientation will be addressed using a quantitative analysis in the following paragraph.

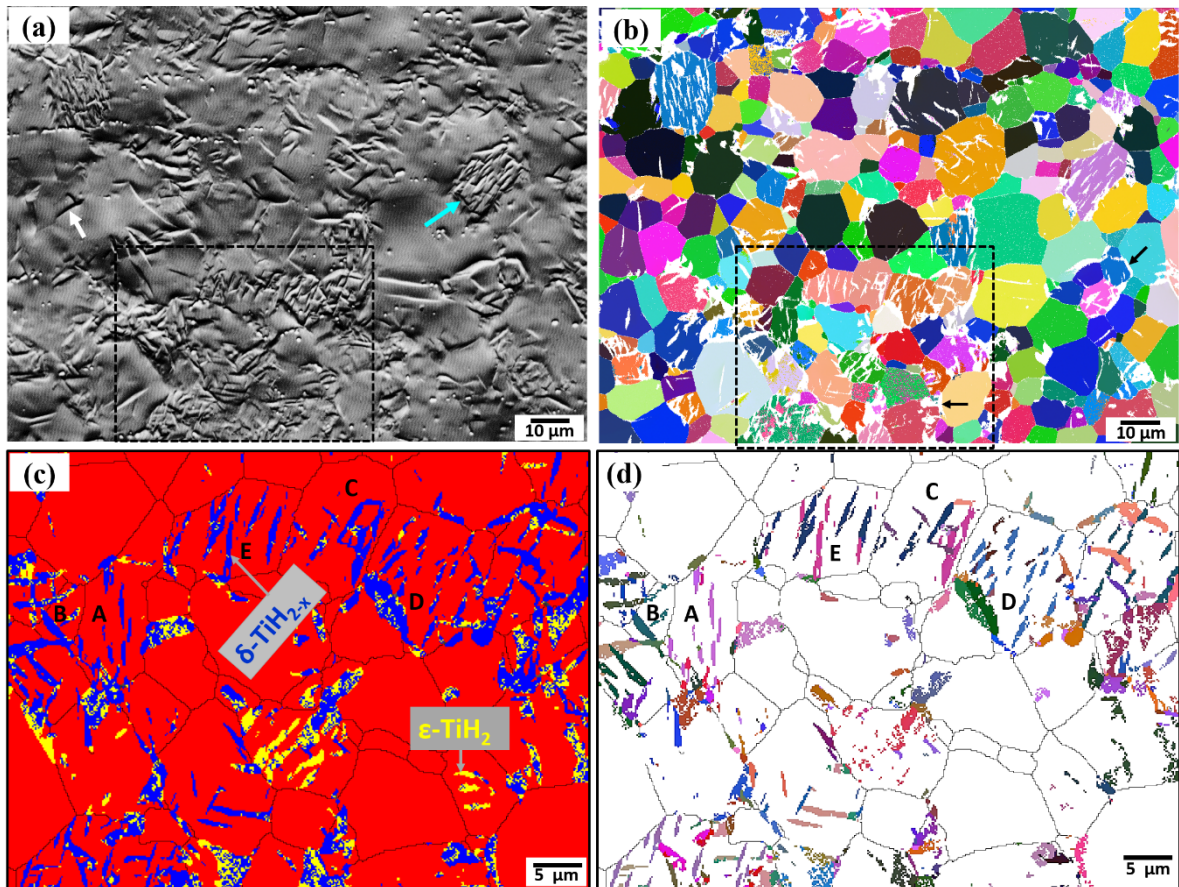


Fig. 3 Hydride characterization of Ti50A-H using high-angular resolution SEM-EBSD. (a) SEM-BSI of Ti50A-H; (b) Euler angles map of α -matrix (hydride indicated by white); (c) Phase map of the selected rectangular area in (b) taken at a smaller step size of $0.10\ \mu\text{m}$ (the α , $\delta\text{-TiH}_{2-x}$ and $\epsilon\text{-TiH}_2$ phase indicated by red, blue and yellow, respectively.) and (d) Euler angles map of FCC hydride $\delta\text{-TiH}_{2-x}$ corresponding to phase map (c).

To further inspect the distribution characteristics of hydrides, microstructure characterization using a high-angular resolution EBSD was performed in the hydrogenated Ti50A-H, as shown in Fig. 3. Due to necessary sample preparation for the EBSD measurement, a layer of

approximately 10 μm thick was removed from the top surface by electropolishing. Fig. 3a displays the backscattered image (BSI) of the interest area, further revealed the two types of hydride distribution: the cluster of hydrides and the isolated hydride, as indicated by green and white arrow, respectively. Fig. 3b presents an Euler angles ($\varphi_1, \Phi, \varphi_2$) map of the matrix α phase taken on the sub-surface of a hydrogenated Ti50A-H sample (the extreme surface has been removed by electropolishing due to EBSD sample preparation), the hydride phases are outlined by white. As observed, most of the plate-like hydrides are grown either isolate or in groups in the interior of α grain. Nevertheless, a low number fraction of hydrides was precipitated along grain boundaries, as indicated by black arrows. Fig. 3c shows the phase map corresponding to the selected rectangle in Fig. 3a and b, which has been taken at a smaller step size of 0.10 μm (the α , $\delta\text{-TiH}_{2-x}$ and $\varepsilon\text{-TiH}_2$ phase indicated by red, blue and yellow, respectively). The Euler angles ($\varphi_1, \Phi, \varphi_2$) map of the δ -hydride (TiH_{2-x} , FCC) from the same area is shown in Fig. 3d. As known, phase transformation from titanium into titanium hydride always follows specific orientation relationships (ORs) [4-15]. As a phase transformation path, the OR usually ensures a minimum lattice deformation for the structure change [31]. Since the δ -hydride is a stable phase [4-6] and that it can be well identified by EBSD technique, the current work is focused to determine the crystallographic ORs between the δ -hydride and the α -phase and their correlation with the hydrides distribution. The A, B, C, D and E grains were used as examples to resolve the ORs and the interface planes in the hydrogenated samples Ti50A-H.

3.2 Determination of orientation relationships and their interface planes between FCC-hydride and HCP-titanium

With an accurate detection of the Euler angles ($\varphi_1, \Phi, \varphi_2$) for each pixel (a disorientation of $\pm 5^\circ$ was considered), the crystallographic ORs represented by the stereographic projections of the corresponding OR plane and OR direction of the two phases, as shown in Fig. 4, were determined by the rotation matrix using the MatLab program. In the pole figures, the poles of the matrix and the δ -hydride are represented with the consistent colors in Fig. 3b and d; the coincidence of projections of the matrix α and δ -hydride is indicated by black frame. This enable us to show that, for example in the A grain, one $\{001\}_\delta$ plane of the δ -hydride was paralleled to one $\{0001\}_\alpha$ plane of the α -matrix; and the projection of one $\langle 110 \rangle_\delta$ direction corresponding to the δ -hydride overlapped one $\langle 1\bar{1}20 \rangle$ projection of the α -matrix, as indicated by the black rectangle in Fig. 4a. According to the rule that the matching directions must be contained in the matching planes, ‘five’ ORs between the δ -hydride and α -matrix

corresponding to the A, B, C, D and E grains were obtained using the stereographic projections, as given in Fig. 4 and Table 1.

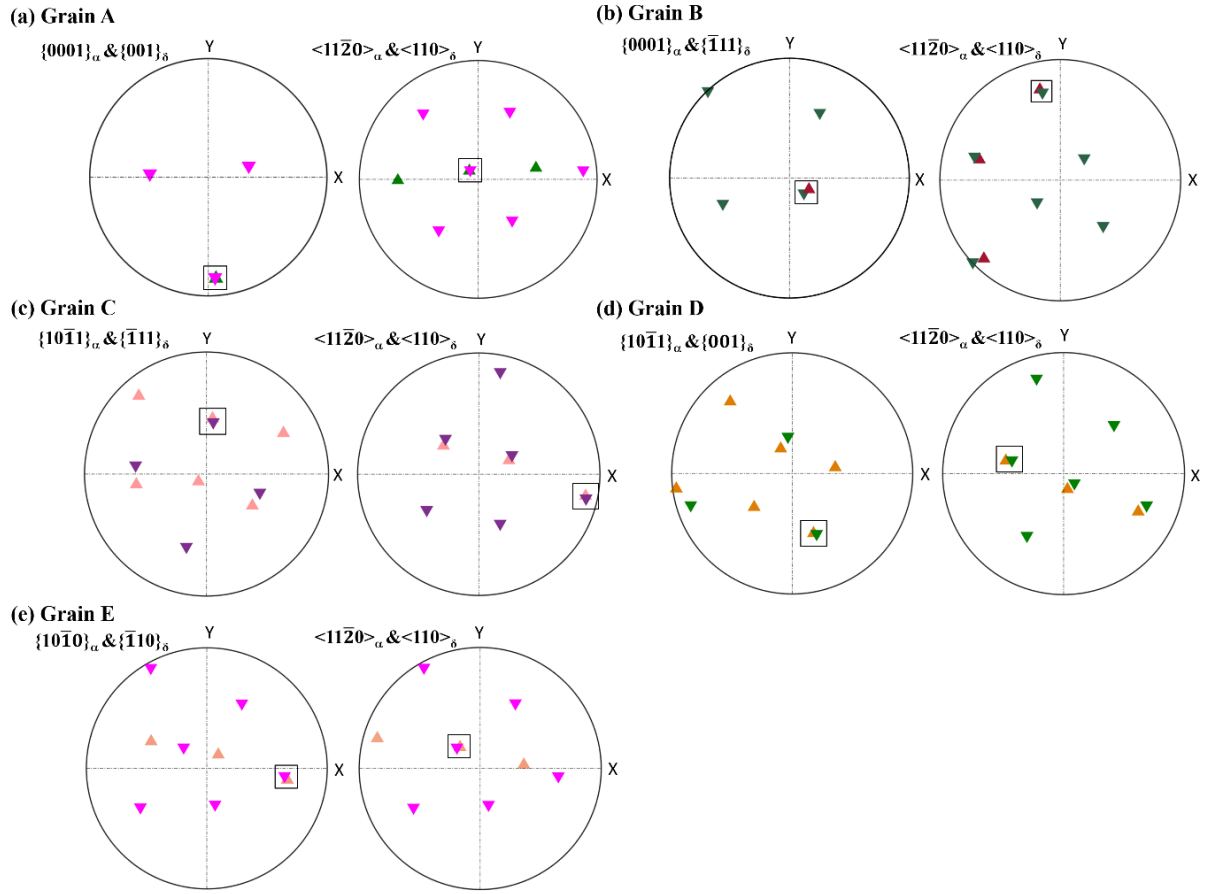


Fig. 4 Stereographic projections of the OR planes and the OR directions corresponding to the matrix α (hcp) and the hydride δ -TiH_{2-x} (FCC) in : (a) A grain, (b) B grain, (c) C grain, (d) D grain and (e) E grain (see Fig.3d). The poles of the matrix and the hydride are represented with the consistent colors in (Fig. 3b and d); the coincidences of the α matrix and δ -hydride projections are indicated by the black frames

The observed ORs in A, B, C and D grains are well consistent with the ones predicted using the edge-to-edge matching model developed by Nie [34] and explored by Zhang et al. [35-37], in which the lowest interatomic spacing misfit along the matching directions and the lowest d-value mismatch between the matching planes were used as the main principle to establish the potential ORs between FCC and HCP crystal systems. The edge-to-edge matching model is based on the analysis of atom positions at the interface, in which both the interatomic spacing misfit and d-value mismatch are only related to the lattice parameter of the parent and the product phases. Regarding these observed ORs, one can note that they all have the common OR direction $\langle 11\bar{2}0 \rangle_{\alpha} // \langle 110 \rangle_{\delta}$, which satisfies the lowest interatomic spacing misfit along the matching directions. It is worth noting that, unlike the OR directions, the OR planes may be rotated a few degrees relative to each other about the OR directions, and therefore, their

relationship cannot be expressed as an exact parallelism. For instance, the observed OR in the B grain does not correspond rigorously to a perfect parallelism between the $\{0001\}$ plane of the hexagonal structure and the $\{111\}$ plane of the fcc structure, but an angle of 3.6° could be worked out (Fig. 4b), which is in agreement with previous observations [37, 4]. This phenomenon has been interpreted with the edge-to-edge matching model, in which both phases are oriented in such a way that the Δg vectors of the reciprocal space connecting the g vectors of the two phases are paralleled to each other and perpendicular to the interface plane [37]. For the same phase transformation, different ORs imply that the precipitation of δ -hydride from the matrix occurred via several paths depending on the interface plane on which the hydride nucleated. In the present work, the detected ORs in the A and D grains is well consistent with, respectively, the OR1* and OR4* reported in the literature [4-6]. The ORs observed between the δ -TiH_{2-x} hydride and the α phase in the B, C and E grains seemed to be the new orientation relationships ever reported. However as suggested by Conforto and Caillard [4], these OR planes in the C and E grains could be the interface planes of the OR4* and OR1*, respectively. Following this assumption, a trace analysis by matching the plane trace of δ -hydride with the published interface plane [4] was performed to further identify these ORs and their corresponding interface planes. The results of these analyses are shown in Fig. 5 and summarized in Table 2 (the stars being used to differentiate the already reported ORs* with the new OR).

Table 1 Examples of ‘five’ ORs observed in Grain A, B, C, D and E; The Euler angles corresponding to the α and the δ -hydride phase in Grain A, B, C, D and E expressed in Bunge’s notation [32, 33]; (The Euler angles listed in this table represent the mean orientation of the α matrix and δ -TiH_{2-x} hydride, respectively.)

Grain ID.	Phase	Euler angles ($\varphi_1, \Phi, \varphi_2$)	Parallel planes and directions between two phase α -Ti and δ -TiH _x
Grain A	α -Ti δ -TiH _x	(4.32, 81.16, 7.85) (105.82, 39.04, 74.77)	$\{0001\}_\alpha // \{001\}_\delta$ & $\langle 11\bar{2}0 \rangle_\alpha // \langle 110 \rangle_\delta$
Grain B	α -Ti δ -TiH _x	(59.96, 21.28, 14.78) (222.63, 35.08, 45.54)	$\{0001\}_\alpha // \{\bar{1}11\}_\delta$ & $\langle 11\bar{2}0 \rangle_\alpha // \langle 110 \rangle_\delta$
Grain C	α -Ti δ -TiH _x	(166.3, 110.16, 25.35) (314.34, 10.15, 78.39)	$\{10\bar{1}1\}_\alpha // \{\bar{1}11\}_\delta$ & $\langle 1\bar{2}10 \rangle_\alpha // \langle 110 \rangle_\delta$
Grain D	α -Ti δ -TiH _x	(157.69, 77.61, 8.91) (186.63, 34.17, 12.85)	$\{10\bar{1}1\}_\alpha // \{001\}_\delta$ & $\langle 1\bar{2}10 \rangle_\alpha // \langle \bar{1}10 \rangle_\delta$
Grain E	α -Ti δ -TiH _x	(165.6, 105.27, 37.19) (217.86, 22.51, 48.34)	$\{10\bar{1}0\}_\alpha // \{\bar{1}10\}_\delta$ & $\langle 1\bar{2}10 \rangle_\alpha // \langle 110 \rangle_\delta$

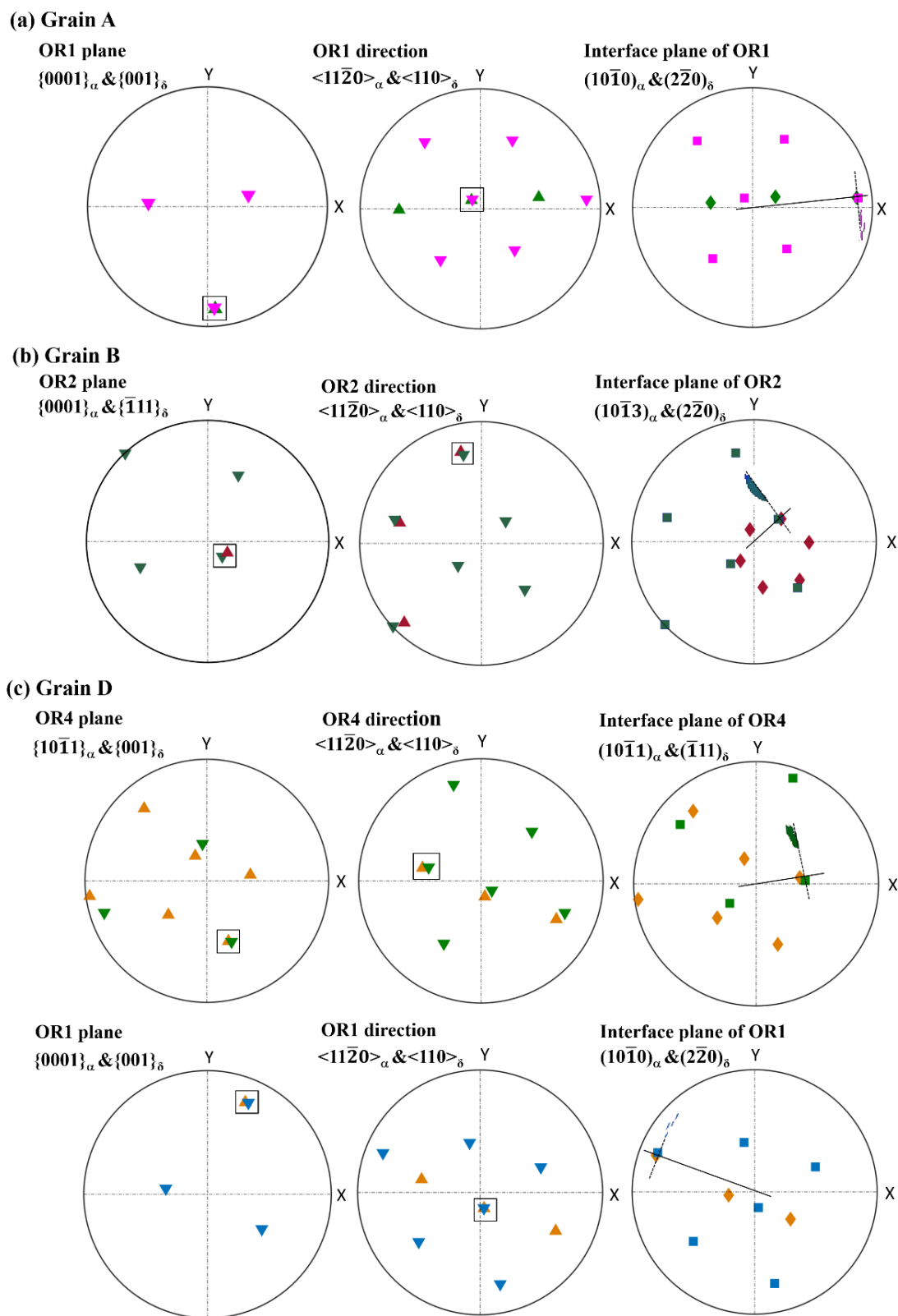


Fig. 5 Stereographic projections of the OR planes, the OR directions and interface planes corresponding to the α matrix (HCP) and the δ -TiH_{2-x} hydride (FCC) in: (a) A grain, (b) B grain and (c) D grain as indicated in Fig. 3c and d. (the coincidence of projections of the α and δ -hydride indicated by black frame, the dash lines outline the surface plane traces of the δ -hydrides and the solid lines connect the center of the pole figures with the poles corresponding to the surface planes and perpendicular to the surface plane traces.)

In the pole figures (Fig. 5), the dash lines outline the surface plane traces of the δ -hydrides and the solid lines connect the center of the pole figures with the poles corresponding to the surface planes of the δ -hydrides and perpendicular to the surface plane traces of the δ -hydrides. For instance, we found that, the ORs and their corresponding interface planes observed in the A and D grains were in complete agreement with the published OR1* and OR4* determined using TEM in Ti40 [4-7, 14, 15], as presented in Fig. 5a, and c, respectively. Meanwhile, the ORs observed in the C and E grains were identified as OR4* and OR1*, respectively. Fig. 5b shows a new OR detected in grain B, which is similar to the one that has been extensively studied in zirconium and its alloys [38-40], it is hereafter called OR2, by analogy with the classification of other authors. It is worth to mention, it is the first time that OR2 is directly observed between δ -hydride (TiH_{2-x} , fcc) and α -Ti in commercially pure titanium, even it has been found in another type γ -hydride (TiH , fct, $c/a=1.19$, formed at very low hydrogen content) [4-7, 11-15]. A further detailed examination for OR2 revealed that, a rotation of 5° could bring OR2 to coincide with OR4*. However, the interface planes corresponding OR2 and OR4* are significantly distinct, which ensures that OR2 is a new OR differing from OR4*.

Table 2 Three ORs and their interface planes observed in Grain A (E), B, and C (D); the area fraction of δ -hydride in each OR; the number fraction of α grains in each OR among the hydrides-contained α grains; and the deviation angle of OR planes.

Grain ID.	Orientation Relationship (OR)	Interface plane	Area fraction of δ -hydride in each OR	Number fraction of α grains in each OR	Deviation angle of OR planes
OR1*					
A and E	$\{0001\}_\alpha // \{001\}_\delta$ $\langle 11\bar{2}0 \rangle_\alpha // \langle 110 \rangle_\delta$	$(10\bar{1}0)_\alpha // (2\bar{2}0)_\delta$	16%	22%	0.05
OR2					
B	$\{0001\}_\alpha // \{\bar{1}11\}_\delta$ $\langle 11\bar{2}0 \rangle_\alpha // \langle 110 \rangle_\delta$	$(10\bar{1}3)_\alpha // (2\bar{2}0)_\delta$	5%	27%	3.62
OR4*					
C and D	$\{10\bar{1}1\}_\alpha // \{001\}_\delta$ $\langle 1\bar{2}10 \rangle_\alpha // \langle \bar{1}10 \rangle_\delta$	$(10\bar{1}1)_\alpha // (\bar{1}11)_\delta$	9%	11%	0.82

OR1* and OR4* have been characterized by TEM in ref. [4].

Looking backward to Fig. 3d, an unignorable observation is that different orientated δ -hydride were formed within one α grain. For instance, the δ -hydrides in OR1* and OR4* coexisted in grain D as evidenced in Fig. 5c, which indicated that several hydrides obeying different ORs can be formed simultaneously or sequentially in one α grain depending on the local hydrogen concentration and the local stress conditions. A statistical analysis (5000 α grains counted) by calculating the area fraction of hydrides in each OR showed that the areas of 26%, 8% and 12%

are occupied by the δ -hydrides in OR1*, OR2 and OR4*, respectively, as summarized in Table 2. The higher fraction of δ -hydrides in OR1* implied that a lower Gibbs energy was required for the nucleation of δ -hydride at the low-energy interface plane $(10\bar{1}0)_\alpha // (2\bar{2}0)_\delta$, even OR2 $\{0001\}_\alpha // \{\bar{1}11\}_\delta$ is supposed to be the most favorable OR with consideration of geometrically matching principals [35-37]. From an energy standpoint, the tetrahedral sites on the $(10\bar{1}0)_\alpha$ planes are the preferential positions for the hydrogen atoms to occupy in the hcp cell [41, 42]. The observed cluster of hydrides in OR1 in the interior of α grains can be therefore attributed to a larger accommodation of hydrogen atoms in the tetrahedral interstitial sites on the $(10\bar{1}0)_\alpha$ plane of hcp lattice as well as in the occupation of the octahedral interstitial sites along the $(2\bar{2}0)_\delta$ plans of the fcc unit cell. On the other hand, the prismatic slip $a/2 \langle 11\bar{2}0 \rangle \{10\bar{1}0\}$ being an easiest slip mode in the α phase, can be readily activated to relax the internal stress generated by the hydride precipitation.

3.3 Hydrides distribution with respect to α grain orientation

Concerning the hydrides-associated fracture phenomenon, it is crucial to examine the distribution of hydrides with respect to grain orientation. To complete the information for the above analysis, the number fraction of α grains (containing δ -hydride) satisfying each OR in all hydride-contained grains (around 2500 α grains) is presented in Table 2. This statistical analysis showed that the α grains containing the δ -hydrides in OR2 were the most frequently observed in the hydrogenated Ti50A-H specimen, signifying that there existed a higher fraction of α grains having a particular orientation, which is believed to facilitate the precipitation of δ -hydrides in OR2. Fig. 6a shows the IPF map of the matrix (α -phase) in the hydrogenated Ti50A-H sample, the δ -hydride TiH_{2-x} is indicated by white. In this IPF map, the α grains in red exhibited a preferential orientation with respect to the ND, their (0002) planes perpendicular to the ND. With respect to the hydrides distribution, the hydrides in the form of clusters located in the interior of α grains were found to satisfy OR1, whereas the isolated hydrides (indicated by black arrows) were obeying OR2. Furthermore, the isolated hydrides in OR2 were formed in the α grains with their [0001] c-axis aligned towards the ND. The observation of the parent α grains with a preferential orientation (in red) with respect to the ND as well as the heterogeneous distributed hydrides throughout the hydrogenated Ti50A-H, highly suggested that there existed a correlation between the hydride precipitation and the α -grain orientation.

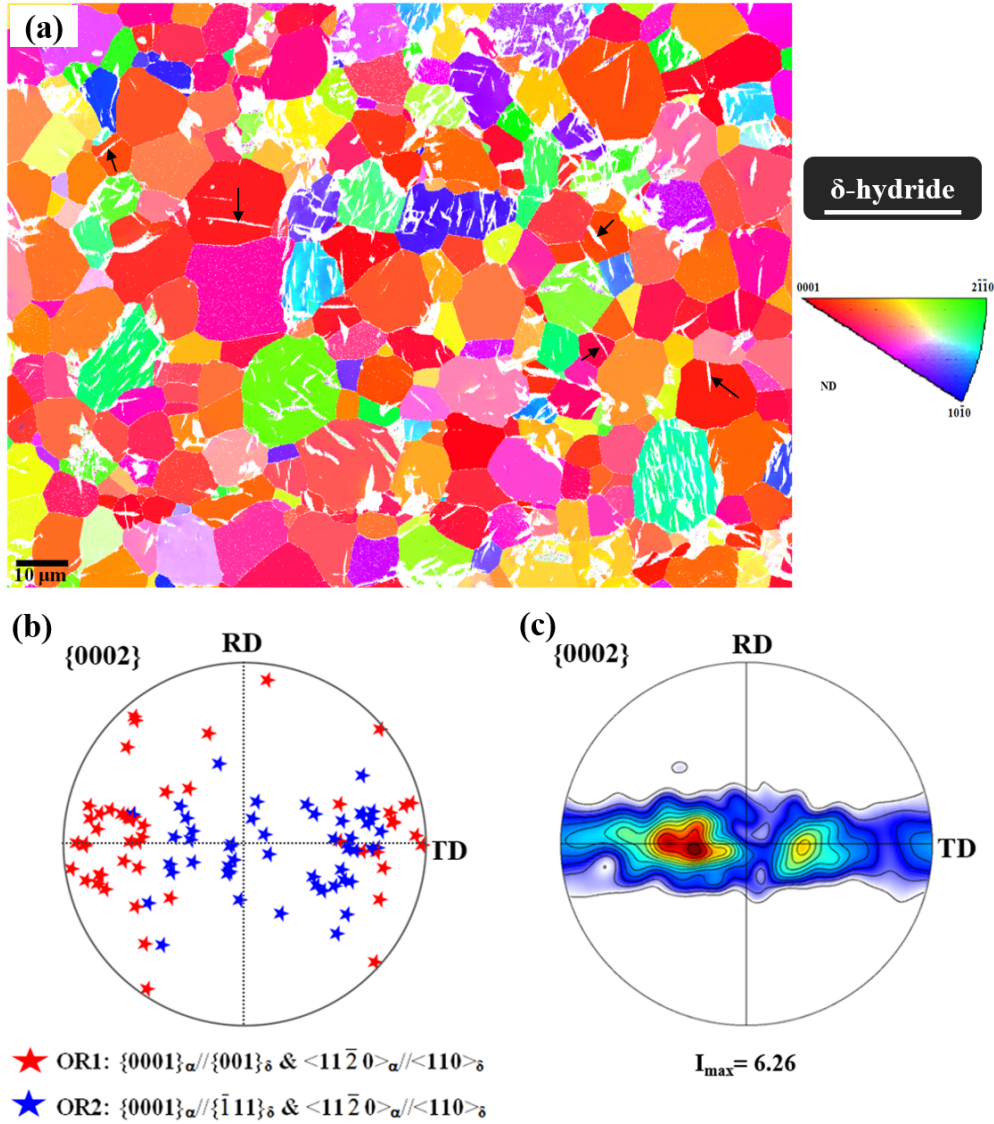


Fig. 6 Correlation between hydride precipitation and grain orientation. (a) IPF map of the matrix of the Ti50A-H, the δ -hydride (TiH_{2-x}) indicated by white color; (b) $\{0002\}$ pole figure of grains following OR1 and OR2; (c) $\{0002\}$ pole figure of AR-Ti50A.

As the OR1 and OR2 are the most frequent ORs observed in the hydrogenated Ti50A-H samples, Fig. 6b presents the $\{0002\}$ pole figure of α grains displaying the OR1 and OR2 with δ -hydride using a semiquantitative analysis. Fig. 6c shows the $\{0002\}$ pole figure of AR-Ti50A sample prior to hydrogen charging, which is characterized by a TD-split basal texture with a maximum intensity occurring at $\pm 30^\circ$ tilted from the ND to the TD. Such a texture is typical for hot rolled Ti-50A sheets, which cannot be totally removed by the subsequent annealing treatment as documented by several studies [43, 44]. As seen, the crystallographic orientations of the α -grains obeying the OR1 and the OR2 were clearly different: the α -grains in OR2 were characterized by crystallographic orientations closely related to the texture component of the rolled sheet (shown in Fig. 6c), whereas the crystallographic orientations of

the α -grains in OR1 with the δ -hydride were found to be nearly paralleled to the TD. In zirconium alloys, the correlation between the formation of hydrides following OR1 and OR2 and the parent grain orientation has been investigated using microstructure characterization of a hydride blister in Zircaloy-4 [40]. The dependency of the δ -hydride transformation paths on the parent α grain orientation found in the present hydrogenated Ti50A-H, is well consistent with the one addressed in Zircaloy-4 [40]. Compared with the frequently observed OR2 in zirconium alloys, OR2 has been rarely reported between δ -hydride and α grains in commercially pure titanium. Based on the previous studies [4-7, 11-15], instead of OR2, OR1 was the dominant OR presented between δ -hydride and α -Ti grains. In the present work, the clusters of δ -hydrides observed nearly parallel in the interior of α grains obeying OR1, indicating that a lower resistance required for the δ -hydride formation in this orientation relationship. The discrepancies of these observations highlighted that the distributions of hydrides are closely related to the local hydrogen concentration and the local stress condition as well as the parent grain orientations. On the other hand, the texture of δ -hydrides could be predicted using the observed ORs, based on the texture of α -Ti. However, the observation of several ORs (OR1*, OR2 and OR4*) for hydrides formation resulted in the uncertainty of hydride texture reconstruction in the present work.

4. Summary

In this study, the crystallographic ORs and their interface planes between the fcc-hydride and the α -titanium have been thoroughly investigated using the stereographic projections of the corresponding OR plane and OR direction and a trace analysis. Owing to an accurate measurement of the Euler angles for each pixel using a high-angular resolution SEM-EBSD, a total of three ORs, one of them being new ORs closely related to the texture component of the rolled Ti50A-sheet, have been determined in the present work. The interface planes of these observed ORs were identified by a statistical trace analysis. The presence of ORs and their interface planes in the hydrogenated Ti50A-H are accounted for by a geometrical edge-to-edge matching model. Furthermore, the correlation between the hydride precipitation and the grain orientation denoted by the $\{0002\}$ pole figure highlighted the dependency of hydride precipitation on the ORs and the parent grain orientation.

Acknowledgements

This research was supported by the French Ministry of Higher Education and Research. The authors appreciate the discussion with Prof. Emanuel Bouzy and Dr. Chunyang Zhang from

LEM3 on the orientation relationships between bcc and hcp structures. EF acknowledges the France-Korea Partenariat Hubert Curien (PHC) STAR program.

Reference

- [1] G. Lütjering, J.C. Williams, Titanium: Engineering Materials and Processes, Springer, 2003.
- [2] M.J. Donachie, Jr. Titanium: A Technical Guide, second ed., ASM, 2000 204-7586.
- [3] M. Wilde, K. Fukutani, Phys. Rev. B 78 (2008) 115411.
- [4] E. Conforto, D. Caillard, Acta Mater. 55 (2007) 785-798.
- [5] E. Conforto, I. Guillot, X. Feaugas, Philos. Trans. R. Soc. A Math. Eng. Sci. 375 (2017) 20160417.
- [6] X. Feaugas E. Conforto, S. Cohendoz, P. Girault, C. Berziou, TMS 2017 146th Annual Meeting & Exhibition Supplemental Proceedings, (2017).
- [7] D. Banerjee, C.G. Shelton, B. Ralph, J.C. Williams, Acta Metall. 36 (1988) 125-141.
- [8] D. Van Heerden, D. Josell, D. Shechtman, Acta Mater. 44 (1996) 297-306.
- [9] M.J. Casanove, E. Snoeck, C. Roucau, J.L. Hutchison, Z. Jiang, B. Vidal, MRS Proceedings. 343 (1994) 277.
- [10] F.D. Manchester, A.H. San Martin, Phase diagrams of binary hydrogen alloys, ASM International, Ohio, 2000, pp. 238-258.
- [11] H. Numakura, M. Koiwa, Acta Mater. 32 (1984) 1799.
- [12] O.T. Woo, G.C. Weatherly, C.E. Coleman, R.W. Gilbert, Acta Metall. 33 (1985) 1897-1906.
- [13] A. Bourret, A. Lasalmonie, S. Naka, Scr. Metall. 20 (1986) 861-866.
- [14] P. Zheng, M.O. Ruault, D. Fournier, R.G. Saint-Jacques, J. Mater. Sci. Lett 9 (1990) 75.
- [15] C. Zhang, Q. Kang, Z. Lai, Acta Metall. Mater. 42 (1994) 2555-2560.
- [16] I. Guillot, X. Feaugas, M. Clavel, Scr. Mater. 44 (2001) 1011-1017.
- [17] J. Huez, X. Feaugas, A.L. Helbert, I. Guillot, M. Clavel, Metall. Mater. Trans. A. 29 (1998) 1615-1628.
- [18] C.Q. Chen, S.X. Li, K. Lu, Acta Mater. 51 (2003) 931-942.
- [19] C.Q. Chen, S.X. Li, K. Lu, Philos. Mag. 84 (2004) 29-43.
- [20] C.Q. Chen, S.X. Li, H. Zheng, L.B. Wang, K. Lu, Acta Mater. 52 (2004) 3697-3706.
- [21] Y.J. Chen, Y.J. Li, J.C. Walmsley, S. Dumoulin, S.S. Gireesh, S. Armada, P.C. Skaret, H.J. Roven, Scr. Mater. 64 (2011) 904-907.
- [22] J. Wen, N. Allain, E. Fleury, in: V. Venkatesh, et al., (Eds.), Proceedings of the 13th World Titanium Conference TMS 2016, pp. 275-280.

- [23] Y.Z. Chen, H.P. Barth, M. Deutges, C. Borchers, F. Liu, R. Kirchheim, *Scr. Mater.* 68 (2013) 743-746.
- [24] J. Wen, N. Allain, E. Fleury, *Mater. Charact.* 121 (2016) 139-148.
- [25] G. Nolze, V. Geist, *Cryst. Res. Tech.* 39 (2004) 343-352.
- [26] G. Miyamoto, N. Takayama, T. Furuhashi, *Scr. Mater.* 60 (2009) 1113-1116.
- [27] T. Wang, F. Eichhorn, D. Grambole, *Phys. Condens. Matter* 14 (2002) 11605-11614.
- [28] Y. Liu, W. Xiang, G. Zhang, B. Wang, *Appl. Surf. Sci.* 285 (2013) 557-563.
- [29] H.L. Yakel, *Acta Cryst.* 11 (1958) 46-51.
- [30] J.C. Williams, Effect of hydrogen on behavior of materials, in: A. W. Thompson, I. M. Bernstein (Eds.), *AIME*, New York, 1976, pp. 367-380.
- [31] M. Liu, Y. Zhang, X. Wang, B. Beausir, X. Zhao, L. Zuo, C. Esling, *Acta Mater.* 152 (2018) 315-326.
- [32] H.J. Bunge, C. Esling, J. Muller, *J. Appl. Cryst.* 13 (1980) 544-554.
- [33] H.J. Bunge, C. Esling, J. Muller, *Acta Cryst. A* 37 (1981) 889-899.
- [34] J.F. Nie, *Acta Mater.* 52 (2004) 795-807.
- [35] M.X. Zhang, P.M. Kelly, M.A. Easton, J.A. Taylor, *Acta Mater.* 53 (2005) 1427-1438.
- [36] M.X. Zhang, P.M. Kelly, *Scr. Mater.* 52 (2005) 963-968.
- [37] M.X. Zhang, S.Q. Chen, H.P. Ren, P.M. Kelly, *Metall. Mater. Trans. A Phys. Metall. Mater. Sci.* 39 A (2008) 1077-1086.
- [38] B. Nath, G.W. Lorimer, N. Ridley, *J. Nucl. Mater.* 49 (1974) 262-280.
- [39] M.A. Vicente Alvarez, J.R. Santisteban, G. Domizzi, J. Almer, *Acta Mater.* 59 (2011) 2210-2220.
- [40] F. Long, D. Kerr, G. Domizzi, Q. Wang, M.R. Daymond, *Acta Mater.* 129 (2017) 450-461.
- [41] R. Khoda-Bakhsh, D.K. Ross, *J. Phys. F: Met. Phys.* 12 (1982) 15-24.
- [42] C. Domain, R. Besson, A. Legris, *Acta Mater.* 50 (2002) 3513-3526.
- [43] Y.B. Chun, S.H. Yu, S.L. Semiatin, S.K. Hwang, *Mater. Sci. Eng. A.* 398 (2005) 209-219.
- [44] S. V. Zharebtsov, G.S. Dyakonov, A.A. Salem, S.P. Malysheva, G.A. Salishchev, S.L. Semiatin, *Mater. Sci. Eng. A.* 528 (2011) 3474-3479.